NANO LETTERS

2006
Vol. 6, No. 5
1000−1006

Self-Sensing Micro- and Nanocantilevers with Attonewton-Scale Force Resolution

J. L. Arlett, J. R. Maloney, B. Gudlewski, M. Muluneh, and M. L. Roukes*

Kavli Nanoscience Institute and Departments of Physics, Applied Physics, and Bioengineering, California Institute of Technology, 114-36, Pasadena, California 91125

Received February 6, 2006; Revised Manuscript Received March 9, 2006

ABSTRACT

Thin, piezoresistive silicon cantilevers are shown to provide unprecedented sensitivity for force detection in an integrated, self-sensing, readily scalable configuration. The devices realized herein are patterned from single-crystal Si epilayer membranes utilizing bulk micro- and nanomachining processes. We demonstrate an electrically transduced force sensitivity of 235 aN/Hz$^{1/2}$ at room temperature and 17 aN/Hz$^{1/2}$ at 10 K. Enhancement of the p+ piezoresistive gauge factor is observed at cryogenic temperatures. The results are employed to elucidate the ultimate, low-temperature sensitivity attainable from self-sensing nanoelectromechanical systems utilizing displacement transduction based upon semiconducting piezoresistors.

Silicon microscale and, more recently, nanoscale cantilevers enable important applications such as atomic force microscopy (AFM) and biological force spectroscopy. Most efforts in these areas employ cantilever probes with *external* displacement transduction via off-chip sensing systems. These systems are typically optically based, involving simple optical beam deflection or more sensitive interferometry. Self-sensing cantilevers, which possess integrated displacement transducers, offer important advantages that are not attainable with external optical methods. Perhaps most prominent are: a) scalability to extremely small cantilever dimensions (far below an optical wavelength) and, thereby, to very high frequencies, b) measurement without optical perturbation of susceptible samples, c) suitability for large-array technologies and portable sensing, and d) ease of applicability to multiple-cantilever sensors that permit correlated or stochastic detection.[1] Furthermore, use of on-chip electronic readout is especially advantageous for detection in liquid environments of low or arbitrarily varying optical transparency, as well as for operation at cryogenic temperatures where maintenance of precise optical component alignment becomes problematic.

Emerging forefront applications such as magnetic resonance force microscopy of single spins[2] and BioNEMS (biofunctionalized nanoelectromechanical systems) for single-molecule biosensing[1] require compliant mechanical nanosensors with force sensitivity at the thermodynamic limit. A milestone along the path toward ultralow noise, self-sensing devices is the work of Harley and Kenny who demonstrated piezoresistive microcantilevers achieving a force noise spectral density of 8.6 fN/Hz$^{1/2}$ in air at a frequency of ~1 kHz with extremely compliant 30 μN/m devices.[3] More recently, Bargatin et al. report measurements of piezoresistive nanocantilevers operating at very high frequencies, up to ~71 MHz, attaining a force sensitivity of 350 aN/Hz$^{1/2}$ in vacuum at room temperature.[4] In this work we demonstrate self-sensing cantilevers with greatly improved sensitivity, and for the first time, we explore the ultimate limits to the performance of such devices that can be expected at low temperatures where thermal noise is small. In addition to studying the temperature dependence and force sensitivity of such devices, we characterize the piezoresistive gauge factor, G, for silicon from cryogenic to room temperature. Previous studies of G have focused upon just a few temperatures[5] or solely explored the range above 50 K.[6]

Our small cantilevers employ high sensitivity piezoresistive strain sensing based upon an integrated semiconducting epilayer. This embodiment of electrical displacement transduction opens a wide parameter space permitting ultrasmall scale, very low stiffness, and very high frequency devices—a regime not approachable via conventional optical detection. This transduction method is also well suited for scaled-down versions of complex detection schemes, such as that of Chui et al., which enables independent resolution of both vertical and lateral forces.[7]

Below we present a detailed method of fabrication for membrane-derived piezoresistive cantilevers based upon bulk micro- and nanomachining processes and provide an experimental and theoretical evaluation of their performance. A scanning electron microscope (SEM) image of a typical device is shown in Figure 1a; the cantilevers are situated at the top of a deep-etched “fluidic via” through the substrate,

* Corresponding author: roukes@caltech.edu.

10.1021/nl060275y CCC: $33.50 © 2006 American Chemical Society
Published on Web 04/18/2006

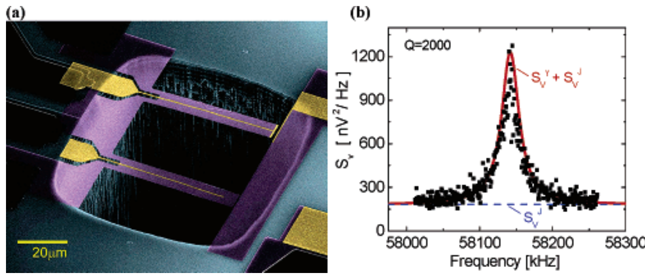

Figure 1. Piezoresistive nanocantilever force sensor. (a) SEM image of the cantilever device with thickness 130 nm, of which the topmost 30 nm comprises the p+ transducer layer. The current path flows along the two outer silicon "legs"; the central Au-coated Si "line" running longitudinally along the center of the device enables biosensing applications.[1] (b) Voltage noise spectral density obtained at room temperature with a 0.3 V bias, measured at the device output terminals. The two principal components evident originate from electrical-domain (Johnson) noise from the transducer itself, S_V^J, and piezoresistively transduced thermomechanical fluctuations, S_V^γ.

a configuration devised for embedding the devices within microfluidic systems for biosensing applications.[1] In this Letter we describe characterization of such cantilevers in vacuo, carried out from room to cryogenic temperatures, to demonstrate the utility of the devices for ultrasensitive force detection. Fabrication begins with a bonded silicon on insulator (SOI) wafer comprised of a 100 nm thick structural layer of undoped silicon, beneath which is a 750 nm sacrificial layer of silicon dioxide (SiO_2). On top of this a 30 nm thick doped Si transducer layer is epitaxially grown, which has a boron doping level of $4 \times 10^{19}/\mathrm{cm}^3$. Above this, 60 nm thick gold electrodes are patterned (each with a 5 nm chromium underlayer to promote adhesion); these form Ohmic electrical contacts to the doped silicon epilayer. A membrane from which the devices are subsequently patterned is created by a backside deep reactive ion etch to form a deep trench through the substrate (75 μm $\times$ 75 μm cross section). This etch is carefully terminated at the oxide layer and ultimately yields the aforementioned fluidic via (Figure 1a). The wafers are then diced into individual 11 mm $\times$ 11 mm dies. Prior to the nanofabrication steps the oxide layer is removed from the backside of the trenches using a buffered oxide etch. The cantilevers are then defined by electron beam lithography, employing lift-off to pattern a 30 nm aluminum mask for protection of the active areas during the subsequent, vertical electron cyclotron resonance plasma etch process using the gases NF_3, Cl_2, and Ar that defines the devices. The aluminum mask is subsequently removed using a 10% potassium hydroxide solution.

These devices have a geometry that is somewhat more complex than a simple cantilever; they are attached to the supports by two small "legs" which serve to concentrate both strain and current flow within the same region to enhance sensitivity (Figure 1a).[3] The completed devices employed in the present study have dimensions $l = 55\ \mu$m, $w = 7\ \mu$m, $w_{\mathrm{leg}} = 2\ \mu$m, and $l_{\mathrm{leg}} = 5\ \mu$m. Much smaller devices have been patterned; this methodology has proven well-suited to fabrication at the sub-100-nm scale. Assuming end-loading and fundamental mode response, the force constant for these devices can be approximately represented as

$$K_0 = \frac{Et^3}{\frac{4l^3}{w} + (2l_{\mathrm{leg}}{}^3 - 6ll_{\mathrm{leg}}{}^2 + 6l^2 l_{\mathrm{leg}})\left(\frac{1}{w_{\mathrm{leg}}} - \frac{2}{w}\right)} \quad (1)$$

Assuming a Young's modulus of $E = 110$ GPa,[8] we deduce from eq 1 a value $K_0 = 2.34$ mN/m for the device of this study. This value is closely confirmed by finite-element numerical simulations[9] which yield $K_0 = 2.46$ mN/m. The effect of the gold electrode patterned along the center of the device has been included in these simulations. These devices are oriented so that current flow within the legs occurs along the $\langle 110 \rangle$ direction for which the piezoresistive coefficient, π_l, is $\sim 4 \times 10^{-10}\ \mathrm{Pa}^{-1}$.[10,11] As grown, the p+ transducer layer has a measured resistivity of 1 kΩ/square; an increase of $\sim$25% was noted after processing. The total two-terminal resistance of the device was 19.3 kΩ. This resistance comprises three contributions: 6.3 kΩ from the strain sensing leg region, 5.5 kΩ/leg for the resistance from the contact pad to the cantilever legs (measured on a four-terminal device of comparable geometry), and 2 kΩ from the spreading resistance at the neck of the cantilever legs and the contribution from the end region of the cantilever.

We now analyze the noise performance of these devices that, ideally, should be limited by the thermomechanical (mechanical-domain) noise of the force sensor itself. We characterize the device noise via $S_F(f)$, the force spectral density with units (force)^2/Hz, which is defined as the Fourier transform of the autocorrelation function of the fluctuating (time-dependent) effective force at the cantilever tip. The "force sensitivity" is then given by $(S_F(f))^{1/2}$ (units of force/Hz$^{1/2}$). The total root mean square force noise is the integral of this force sensitivity over the measurement bandwidth. The force spectral density arising from thermomechanical fluctuations, which is white over the physically relevant regime, is given by $S_F^\gamma = 4k_BT\gamma = 4k_BTK_0/(2\pi Qf_0)$. Here γ, f_0, and $Q = 2\pi M_0 f_0/\gamma$ are the damping coefficient (with units kg/s), fundamental mechanical resonance frequency, and quality factor, respectively, for the vibrational mode under consideration. $M_0 = K_0/(2\pi f_o)^2$ defines the modal mass. At room temperature the measured fundamental resonance frequency and quality factor are 58.1 kHz and 2000, respectively (Figure 1b); hence the associated force sensitivity expected from thermomechanical fluctuations is 235 aN/Hz$^{1/2}$. The cantilever's dynamical response function, $H(f)$, transforms this force spectral density into the spectral density for displacement fluctuations

$$S_x^\gamma(f) = S_F^\gamma |H(f)|^2 = S_F^\gamma \frac{1}{16\pi^4 M_0^2[(f^2 - f_0^2)^2 + (ff_0/Q)^2]} \quad (2)$$

Here x represents the coordinate of cantilever motion measured at its distal end.

Other "extrinsic" noise sources affect the device performance. In the absence of force stimuli, thermodynamic

displacement fluctuations are transduced by the biased piezoresistors into an equivalent voltage noise at the device output terminals. In the ideal case, the transduced contribution from $S_x^\gamma(f)$ should dominate the intrinsic, electrical-domain noise of the piezoresistors (arising from Nyquist and flicker-noise mechanisms). More formally, the voltage noise spectral density arising from electrically transduced thermomechanical fluctuations is $S_V^\gamma(f) = S_x^\gamma(f)\mathscr{R}^2(I_b)$. Here $\mathscr{R}(I_b) = I_b(\partial R_T/\partial x)$ represents the voltage responsivity (with units V/m) characterizing the performance of the piezoresistive transducers biased with a dc current, I_b. The quantity $\partial R_T/\partial x$ represents the differential sensitivity of device resistance to displacement; it can be deduced empirically by fitting the electrically transduced thermomechanical resonance peak to a Lorentzian response (Figure 1b), after subtracting the predominantly white background electrical noise near resonance (which we measure experimentally). For the present device this procedure yields $\partial R_T/\partial x \sim 0.017$ Ω/nm. Theoretically we expect this differential responsivity to be given by the expression

$$\partial R_T/\partial x = \frac{3\beta\pi_l}{2w_{leg}t^2}(2l - l_{leg})K_0 R_T \quad (3)$$

where R_T is the resistance of the "sensing region" of the device. (For our two-leg devices finite element simulations show the narrow legs are the regions that both dominate the two-terminal resistance as well as develop the highest strain upon cantilever deflection.) We estimate R_T from the device geometry using the measured resistance per square for the material. β is a parameter introduced by Harley and Kenny to account for the fraction of the full strain distribution sampled by the finite-thickness piezoresistive layer; in their work $\beta \sim 0.7$. We also employ this value of β for our devices, which are geometrically similar.[3] Using eq 3 and the measured $\partial R_T/\partial x$ from Figure 1b, we can deduce the device gauge factor as $G = \pi_l E = 47$. This agrees quite closely with the expected value of 44.[10,11] Similar results were obtained upon performing a direct measurement of the gauge factor using an AFM, which provided a calibrated displacement.

To evaluate the temperature-dependent force sensitivity of the device requires evaluation of the actual device temperature, which can be affected by bias-current-induced heating. As demonstrated below, this begins to play a significant role only at our lowest temperatures and is otherwise negligible. In this regime the electronic carriers (holes) and phonons within a device under bias are not in thermal equilibrium. For the temperature range over which experimental results are presented here ($T_0 \geq 6$ K, where T_0 is the ambient temperature) thermal conduction via hole diffusion is negligible (as confirmed later in this paper). For the purpose of these calculations we therefore assume that all heat is dissipated via the phonon conduction pathway. The temperature dependence of the mechanical properties of the device is determined by the phonon temperature (T_{ph}). We assess this quantitatively by assuming that uniform Joule heating within the cantilever legs along their length generates a one-dimensional phonon temperature profile, satisfying the expression $2tw_{leg}\kappa_{Si}(d^2T_{ph}/dy^2) = -\dot{Q}/l_{leg}$. Here $y = [0,l_{leg}]$ represents the position along a cantilever leg measured from its anchoring support. We assume the thermal boundary condition at $y = 0$ is established by the (regulated) substrate temperature, whereas at $y = l_{leg}$, the distal end of the cantilever legs, it is established by the condition that the temperature gradient vanishes in these vacuum-based measurements. Heat loss via blackbody radiation is negligible. At low temperatures the thermal conductivity of silicon, κ_{Si}, is estimated assuming simple diffusive thermal transport $\kappa_{Si} \sim c_v\bar{v}_s\bar{l}/3 = \alpha_{ph}T_{ph}^3$, where c_v is the specific heat per unit volume given by the Debye formula, $c_v(T) = [12\pi^4k_B\rho/(5m_{si})](T_{ph}/T_D)^3$, m_{si} is the atomic mass of silicon, and $T_D = 645$ K is the Debye temperature for silicon. The average speed of sound for silicon is given by $\bar{v}_s = \langle\sum_{i=1}^3 1/v_i^2\rangle/\langle\sum_{i=1}^3 1/v_i^3\rangle \sim 5634$ m/s (at 73 K), where the summation is over propagation modes and the average is over propagation direction.[12] Here $\bar{l}$ is the effective phonon mean free path. Upon the basis of previous low temperature thermal transport studies of nanoscale beams with geometry similar to the piezoresistive legs employed here,[13] we assume a boundary scattering limited value $\bar{l} \sim 1.12\sqrt{A}$. Here A is the cross sectional area of the beam.[14] With these formulas we deduce the average temperature within the leg region in steady-state (under current bias) for all data taken below 40 K. Above 40 K the Debye formula ceases to be valid for determining thermal conductivity—however, for the full range of biases employed in this work we have verified that bias heating is negligible in this regime. From the thermal diffusion equation we obtain a steady-state temperature profile

$$T_{ph}(y) = (\dot{Q}l_{leg}/2tw_{leg}\alpha_p - \beta^2(y^2/l_{leg}^2 - 2y/l_{leg} + 1))^{1/2}/\beta^{1/2} \quad (4)$$

along the length of the piezoresistors, where $\beta = ((T_0^4 + 2l_{leg}\dot{Q}/tw_{leg}\alpha_p)^{1/2} - T_0^2)/2$ and T_0 is the ambient temperature. We employ its longitudinally averaged value $\langle T_{ph}\rangle = \int_0^{l_{leg}} [T_{ph}(y)/l_{leg}]\, dy$ as an approximate measure of the effective device temperature in steady state.

The cryostat-mounted sample stage was engineered such that a 100 Ω resistor, used for controlling the ambient temperature, passed through the center of a copper block on which the sample was mounted. Apiezon N grease was used to ensure thermal contact of the heating resistor and copper block. A silicon diode thermometer was mounted on the opposite side of the copper block at a comparable distance from the heating resistor as the microcantilever device. The measured temperature from this diode was used as the ambient temperature, T_o. The diode thermometer and heating element were controlled using a Lakeshore 340 temperature controller.

To assess the validity of the effective phonon temperature of the piezoresistive sensors calculated above, we perform two control experiments summarized in Table 1. In the first, we fix the bias power and evaluate the resulting temperature rise in the sensors (piezoresistors) for various ambient (substrate) temperatures, T_0. This procedure involves an

Table 1. Summary of Control Experiments Performed To Assess the Validity of the Heating Correction[a]

$P = 22\ \mu$W			$T_0 = 11.5$ K		
T_0 (K)	ΔT_{meas} (K)	ΔT_{calc} (K)	P (μW)	ΔT_{meas} (K)	ΔT_{calc} (K)
7.6	13.3	12.4	3.4		4.0
11.5	10.4	9.9	6.9	5.9	5.8
15.0	7.8	8.0	22	10.4	9.9
20.0	4.6	5.8	43	12.6	12.9
			47	12.9	13.4

[a] T_0 is the initial temperature (before heating), ΔT_{meas} is the temperature rise as determined by the resonance frequency shift (Figure 2a), and ΔT_{calc} is the temperature rise estimated from the thermal conduction calculations discussed in the text.

initial calibration of the resonant frequency versus substrate temperature, measured using very small bias power (3.4 μW) so that temperature disequilibrium is minimal. Significant local heating is then induced by increasing the bias current so that much more power, 22 μW, is dissipated within the piezoresistors while the substrate is simultaneously regulated at several specific temperatures, T_0. The resulting local temperature rise at the sensors is evaluated by converting the observed resonant frequency shift to sensor temperature (Figure 2a) via the initial calibration. (This procedure is valid since it is the temperature dependence of Young's modulus within the heated leg region that predominantly gives rise to the resonant frequency shift.) This temperature is then compared with the value derived from the heating calculations. In a second experiment we regulate the substrate temperature at 11.5 K and apply four different (relatively large) values of the bias power, as tabulated. A similar procedure is then employed to deduce local sensor temperature. In both cases the agreement between the local temperature rise measured from resonance frequency shifts and that estimated from the aforementioned calculations are within 7% for temperatures up to 15 K and all applied bias powers (up to 47 μW).

With this validation of our procedure for evaluating effective temperature we can confidently deduce the temperature dependence of both the quality factor and gauge factor. These are displayed in parts b and c of Figure 2, respectively. The quality factor is observed to increase from 1900 at room temperature to 10 000 for $T \leq 30$ K. The gauge factor is evaluated over the temperature range from 11 to 300 K by fitting to thermomechanical noise data (using a procedure based upon eqs 2 and 3) after carefully subtracting the electrical noise contributions. Figure 2c shows that the piezoresistive response increases with decreasing temperature, consistent with the few reports that exist in the literature.[5,6] The temperature-dependent thermomechanical noise is shown in Figure 3. A minimum value of 17 aN/Hz$^{1/2}$ is attained at an effective device temperature of 10.4 K (inset).

Apart from the high force sensitivity we have attained, perhaps the most compelling aspect of our present results is that they can be employed to elucidate the ultimate limits of semiconductor-based piezoresistive displacement sensing for NEMS. Specifically we can evaluate: (a) the lowest temperatures at which piezoresistive displacement transduction remains useful, (b) the optimal bias current for a given ambient temperature, and (c) the ultimate force sensitivity that is attainable with piezoresistive cantilevers at low temperatures where optimal performance is obtained. The analysis proceeds as follows. The transduction responsivity of a piezoresistive cantilever, $\mathscr{R}(I_b)$ is proportional to the bias current applied through the device—but this, in turn, also determines the power dissipated within the piezoresistors, $P_{in} = I_b^2 R_T$. This power input, in turn, induces a temperature rise determined by the thermal conductance available from all mechanisms that serve to cool the piezoresistors. In steady state, a temperature $\langle T^*(T_0,I_b)\rangle$ is thereby established, which depends on the ambient temperature, T_0 and applied bias, I_b. We view T_0 as the independent variable since its value is typically dictated by the sensing application. Hence, for a given T_0 there exists an optimal bias current, $I_b^{(opt)}(T_0)$, that yields the optimum force sensitivity, $\sqrt{S_F(T_0)}|_{opt}$, at that temperature. However, below a characteristic temperature $T_0 < T_0^{(min)}$, the steady-state device temperature, $\langle T^*(T_0,I_b)\rangle$, is predominantly determined by Joule heating, and *not* by the ambient temperature T_0. In the previous analysis a single pathway for dissipation of bias-induced Joule heating was considered, namely, heat transfer from holes to the phonon bath and then to the environment via phonon transport. A second potential pathway for heat dissipation is available, specifically hole diffusion along the electrical conductors. These two mechanisms for thermal conduction act in parallel, as schematically depicted in Figure 4. For the analysis here (which extends to lower temperatures than the experimental data presented earlier) we must consider both pathways. In doing so we will explicitly justify the omission of the hole diffusion pathway in the earlier analysis of our data at higher temperatures, $T \geq 6$ K.

Here we evaluate the effective steady state for the phonons and holes in the strain sensing region of the device, making it possible to evaluate the total force spectral density on resonance, referred to input (RTI). This is given by the formula

$$S_F = S_F^{\gamma} + S_F^{J} = \frac{2k_B K_o}{\pi f_o Q}\int_0^{l_{leg}} \frac{T_{ph}}{l_{leg}}\,dy + \frac{4k_B R_T}{\mathbf{T}^2}\int_0^{l_{leg}} \frac{T_h}{l_{leg}}\,dy \tag{5}$$

where S_F^{γ} is the thermomechanical noise and $S_F^{J} = S_V^{J}/\mathbf{T}^2$ is the (Johnson) electrical noise (RTI). Here $\mathbf{T} = \mathscr{R}(Q/K_o)$ is the ganged system responsivity, the product of the transducer and on-resonance mechanical responsivities, $S_V^{J} = 4k_B T_h R_T$ is the (Johnson) voltage noise of the transducers and T_h is the effective temperature of the holes. Note the separate roles played by the phonon and hole temperatures for the mechanical and electrical degrees-of-freedom, respectively.

The calculation proceeds as follows. The temperature profile for the holes is solved for using the diffusion equation; $2t_{doped}w_{leg}\kappa_h(d^2T_h/dy^2) = -\dot{Q}_h/l_{leg}$ where the hole thermal conductivity is given by the Widemann−Franz law $\kappa_h = \pi^2(k_B/e)^2\sigma T_h/3$. The temperature dependence of the thermal conductivity makes solution of this differential equation

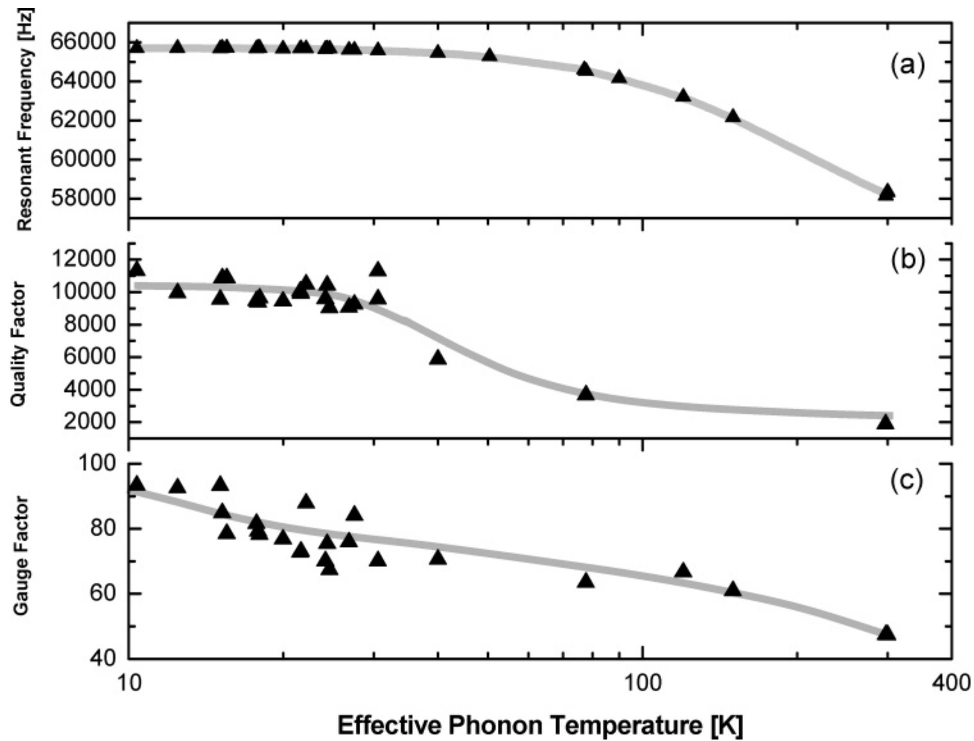

Figure 2. Temperature-dependent performance of nanocantilever force sensor: (a) resonance frequency; (b) quality factor; and (c) gauge factor. The data are for the thermomechanical resonance, collected at a bias of 3.3 μW. The temperature scale has been corrected to account for heating at this bias power as discussed in the text. The solid gray lines provide a guide to the eye.

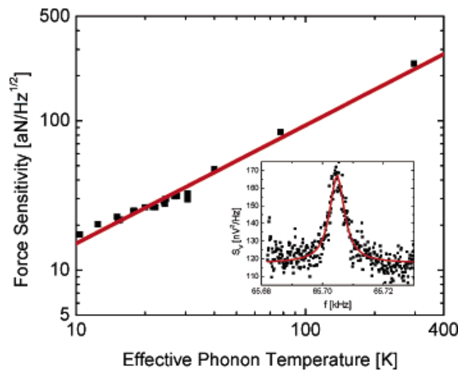

Figure 3. Force noise spectral density for the nanocantilever force sensor. The temperature-dependent magnitude of the thermomechanical force noise is shown here. Over the range shown, the data follow an approximately linear trend; a least-squares fit yields a $T^{0.8}$ dependence (solid line). Inset: The measured voltage noise at a device temperature of 10.4 K.

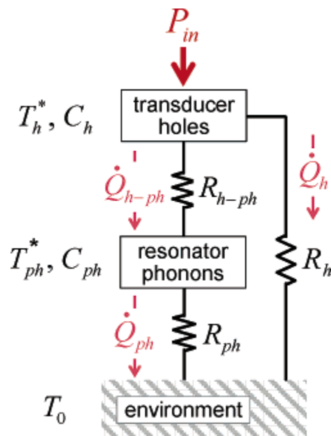

Figure 4. Model for low temperature thermal transport in semiconducting piezocantilevers. Joule heating of the transducer's hole gas arising from the applied bias, P_{in}, is dissipated by both phonon emission, $\dot{Q}_{h-ph}$, and hole diffusion down the electrical leads to the environment (i.e., substrate), $\dot{Q}_h$. The induced heating of the resonator phonons is subsequently dissipated into the environment via phonon transport, $\dot{Q}_{ph}$. The thermal resistances characterizing these processes are R_{h-ph}, R_h, and R_{ph}, respectively. In steady state, with the environment at temperature T_0, this branched heat flow raises the hole gas and resonator phonon temperatures to T_h* and T_{ph}*, respectively. The heat capacities of the hole gas and resonator phonons are C_h and C_{ph}, respectively.

nontrivial; hence we evaluate it numerically. In these equations T_h represents the (local) effective steady-state temperature of the holes, t_{doped} represents the thickness of the conducting layer of the piezoresistor, σ represents the conductivity of the piezoresistor, and e is the electronic charge. The temperature profile of the phonons is determined by eq 4 where the heat transferred, $\dot{Q}$, is now $\dot{Q}_{ph}$, the heat transferred via the phonon conduction pathway.

Once the temperature profiles for holes and phonons have been evaluated, the heat transferred from holes to phonons can be calculated using the equation, $\dot{Q}_{h-ph} = \int dV \int_{T_{ph}}^{T_h} dT\, G_{h-ph}(T(y))$, where the volume integral is over the conducting region of the device and G_{h-ph} is the hole−phonon thermal conductance per unit volume given by $G_{h-ph}(T) = C_h(T)\Gamma_{h-ph}(T) = g_{h-ph}T^4$, where C_h is the electronic heat capacity per unit volume and Γ_{h-ph} is the hole−phonon scattering rate.[15] We model the hole heat capacity as that of Sommerfeld free hole gas, $C_h(T) = \pi^2 p k_B{}^2 T/\epsilon_F = \gamma_h T$, where p is the hole density, $\epsilon_F = \hbar^2(3\pi^2 p)^{2/3}/2m_h$ is the Fermi energy, and m_h is the (light)

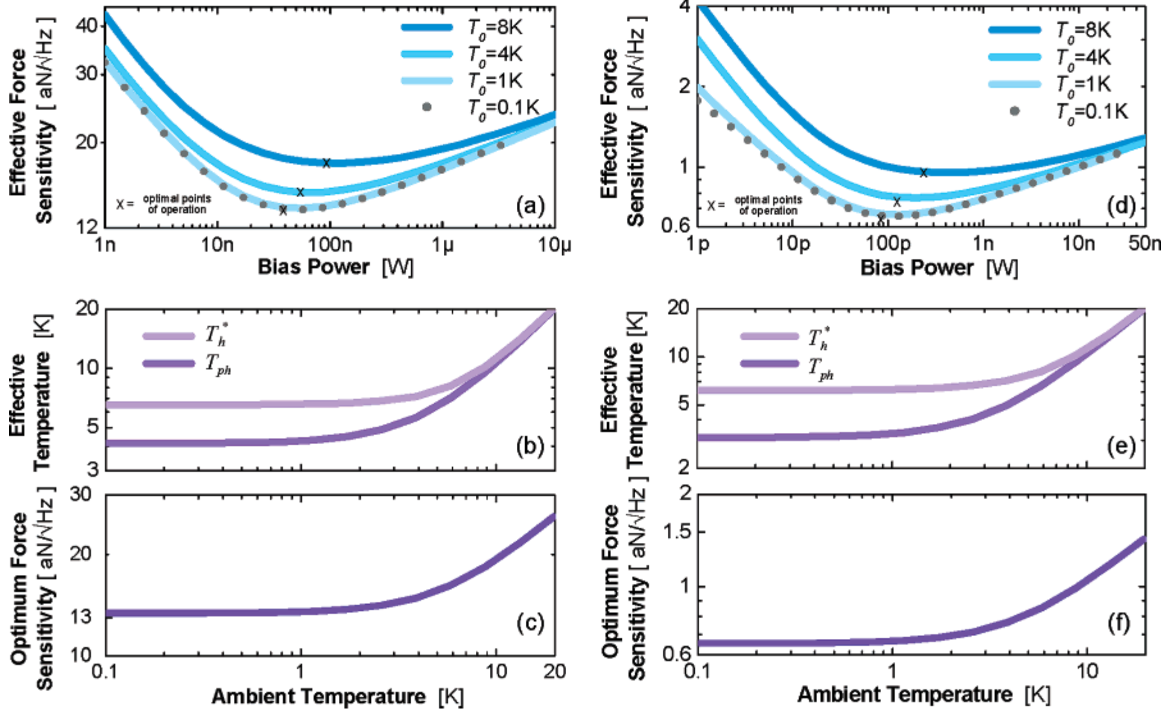

Figure 5. Optimization of transduced force sensitivity. (a, d) Evaluation of the bias power dependence of the effective force noise, which includes both mechanical and electrical domain contributions (referred to input). Calculated performance is displayed for two device geometries (see text): the microdevice on which experiments were conducted in this paper (plots a, b, and c) and a smaller, but realistic, nanodevice (plots d, e, and f). At each ambient temperature, T_0, the minima define an optimal bias point, $P_{in}^{(opt)} = I_B^{(opt)}R_T^2$. At low bias power the responsivity of the transducer decreases, thereby leading to an increase in the effective force noise (referred to input). At high bias power the total force noise increases due to Joule heating. (b, e) At the optimal bias power the transducer hole gas and the resonator phonons attain elevated steady-state temperatures, T_h^* and T_{ph}, which depend on T_0. (c, f) The optimum force sensitivity attained at $P_{in}^{(opt)}(T_0)$ is shown as a function of T_0. Note that an improvement in force sensitivity of greater than an order of magnitude is observed for the nanoscale device.

hole mass in the valence band. Assuming the holes and phonons are Fermi and Bose distributed, respectively, the deformation potential hole−phonon scattering rate, Γ_{h-ph}, is given by $\Gamma_{h-ph} = (3\varsigma(3)k_B^3D^2/\pi\hbar^4\bar{v}_s^4v_F\rho)T^3 = \alpha_{h-ph}T^3$, where $D = 8.3$ eV is the deformation potential[16,17] and $\varsigma(3) = 1.202$. The relative values for the heat conducted via the two thermal conduction pathways $\dot{Q}_h$ and $\dot{Q}_{ph}$ is not known a priori. The system is solved iteratively until convergence is attained, yielding $\dot{Q}_{h-ph} = \dot{Q}_h$ (subject to the constraint $P_{in} = \dot{Q}_h + \dot{Q}_{ph}$).

The effective, electrically transduced force noise RTI calculated with this model is shown at four different ambient temperatures in Figure 5a for the experimental device geometry. For very low bias currents, the total force noise increases due to the smaller transducer responsivity and consequently the dominance of S_F^J (RTI). At high bias currents, the total noise increases due to the increased device temperature. It is clear that by minimizing eq 5 we can determine the optimum bias power, P_{in}, yielding the highest sensitivity for a given ambient temperature and device geometry. The effective temperature of both the phonons and holes is shown in Figure 5b. It is evident that below a few degrees kelvin, the Joule heating is very significant in determining the effective device temperature. The temperature dependence of the optimum force sensitivity obtained by this procedure is shown in Figure 5c for the experimental geometry. The corresponding effective temperatures for the holes and phonons are shown in Figure 5b. As seen, a limiting sensitivity of $S_F^{1/2} = 13aN/\text{Hz}^{1/2}$ can be achieved for an ambient temperature $T_0 < 1$ K.

This analysis allows us to assess the sensitivity improvements possible through optimization of geometry—for example, by reducing the width of the cantilever legs and decreasing the total device thickness. To illustrate the improvements that are easily within the scope of our present, top-down nanofabrication capabilities, we consider nanocantilever devices with $w_{leg} = 100$ nm, $w = 300$ nm, $t = 30$ nm, $t_{doped} = 7$ nm, $l_{leg} = 1$ μm and otherwise identical to the device of Figure 1. For such a device one obtains an optimal sensitivity $S_F^{1/2} = 0.6aN/\text{Hz}^{1/2}$ for $T_0 < 1$ K. A quality factor of 10 000 was assumed for this device. This seems reasonable based on a survey of work that has gone on in the field.[18] The optimum sensitivity versus ambient temperature is shown in Figure 5f.

In the analysis of our experimental data we asserted that thermal conduction via holes was not significant in the temperature range studied. We revisit that assertion here. The lowest temperature of data collection was at an ambient temperature of 6.0 K, with a bias power of 1 μW. Under the assumption that the power was dissipated entirely via the phonon conduction pathway, an average phonon temperature of 10.3 K was calculated. On the basis of this phonon temperature and 1 μW of power transfer, we obtain an effective average hole temperature of 12.8 K. The heat

dissipated via hole diffusion at this effective hole temperature, estimated using the Wiedemann−Franz law, $\dot{Q}_{h-ph} \sim 2\pi^2(k_B/e)^2/3R_T(\langle T_h\rangle^2 - \langle T_0\rangle^2)$, is of order 1 nW and therefore negligible compared to the 1 μW dissipated via phonon conduction.

The results presented here elucidate the ultimate, practical limits for self-sensing displacement transduction by means of semiconducting piezoresistors. We have experimentally demonstrated the attainment of a force noise floor at the level of 17 aN/Hz$^{1/2}$ at $\sim$10 K, a record for self-sensing devices. Furthermore, our analysis establishes that sub-aN/Hz$^{1/2}$ sensitivity is attainable by scaling the cantilever dimensions downward into a regime that is readily attainable by top-down methods. Our analysis also elucidates, for the first time, the existence of a temperature- and geometry-dependent optimum bias current at which the force sensitivity is maximized. This analysis shows that heating effects in micro- and nanoscale piezoresistive devices become substantial for ambient temperatures below 1 K. This would appear to preclude attainment of quantum-limited force sensitivity at temperatures $T_0 \leq \hbar\omega_0/k_B$ where the resonant mode becomes thermally depopulated but otherwise clearly enables a wide range of applications requiring compact and integrated high-frequency force sensing with unprecedented sensitivity.

Acknowledgment. We gratefully acknowledge support for this work from DARPA/MTO through SPAWAR Grant Number N66001-02-1-8914 and from the NSF under ECS-0089061. J.R.M. acknowledges support from a NSF graduate research fellowship. We also thank Tronic's Microsystems S.A., particularly Drs. Peter Pfluger, Natacha Raphoz, Ariel Cao, and Christian Pisella, for a fruitful collaborative work on wafer-scale NEMS fabrication.

References

(1) Arlett, J. L.; Paul, M.; Solomon, J.; Cross, M. C.; Fraser, S. E.; Roukes, M. L. In *Controlled Nanoscale Motion in Biological and Artificial Systems*; Nobel Symposium 131, June 2005; Linke, H., et al., Eds.; Springer-Verlag: Heidelburg, in press.
(2) Rugar, D.; Budakian, R.; Mamin, H. J.; Chui, B. W. *Nature* **2004**, *430*, 6997.
(3) Harley, J. A.; Kenny, T. W. *Appl. Phys. Lett.* **1999**, *75*, 289.
(4) Bargatin, I.; Myers, E. B.; Arlett, J.; Gudlewski, B.; Roukes, M. L. *Appl. Phys. Lett*. **2005**, *86*, 133109.
(5) Yuan, C. W.; Batalla, E.; Zacher, M.; de Lozanne, A. L.; Kirk, M. D.; Tortonese, M. *Appl. Phys. Lett.* **1994**, *65*, 1308.
(6) Morin, F. J.; Geballe, T. H.; Herring, C. *Phys. Rev.* **1957**, *105*, 525.
(7) Chui, B. W.; Kenny, T. W.; Mamin, H. J.; Terris, B. D.; Rugar, D. *Appl. Phys. Lett.* **1998**, *72*, 1388.
(8) Li, X.; Ono, T.; Wang, Y.; Esashi, M. *Appl. Phys. Lett.* **2003**, *83*, 3081−3083.
(9) CFD-ACE, Computational Fluid Dynamics Research Corporation, Huntsville, AL.
(10) Tufte, O. N.; Stelzer, E. L. *J. Appl. Phys.* **1963**, *34*, 313.
(11) Mason, W. P.; Thurston, R. N. *J. Acoust. Soc. Am.* **1957**, *29*, 1096.
(12) Hurst, W. S.; Frankl, D. R. *Phys. Rev.* **1969**, *186*, 801.
(13) Fon, W.; Schwab, K. C.; Worlock, J. M.; Roukes, M. L. *Phys. Rev. B* **2002**, *66*, 045302.
(14) Klitsner, T.; VanCleve, J. E.; Fischer, H. E.; Pohl, R. O. *Phys. Rev. B* **1988**, *38*, 7576.
(15) Little, W. A. *Can. J. Phys.* **1959**, *37*, 334.
(16) Sham, L. J. *Proc. Phys. Soc.* **1963**, *81*, 934.
(17) Aubrey, J. E.; Gubler, W.; Henningsen, T.; Koenig, S. H. *Phys. Rev.* **1963**, *130*, 1667.
(18) Yasumura, K. Y.; Stowe, T. D.; Chow, E. M.; Pfafman, T.; Kenny, T. W.; Stipe, B. C.; Rugar, D. *JMEMS* **2000**, *9*, 117.

NL060275Y